# Operating Characteristics of GaAs/InGaP Self Aligned Stripe Lasers

Benjamin J. Stevens[1], Kristian M. Groom[1], David T. D. Childs[1], Yong Ang[1], Ryan R. Alexander[1], Andrey B. Krysa[1], John S. Roberts[1], Amr S. Helmy[2], and Richard A. Hogg[1]

[1] *Department of Electronic and Electrical Engineering, Centre for Nanoscience and Technology, The University of Sheffield, North Campus, Broad Lane, Sheffield S3 7HQ, United Kingdom*
[2] *Department of Electrical and Computer Engineering, University of Toronto, 10 King's College Rd., Toronto, ON, M5S 3G4, Canada*

Received October 1, 2008; revised November 13, 2008; accepted November 18, 2008; published online April 20, 2009

We demonstrate a novel process for fabrication of GaAs based self-aligned lasers based upon a single overgrowth. A lattice matched n-doped InGaP layer is utilized for both electrical and optical confinement. We present operating characteristics such as external differential quantum efficiency, T-zero and far field as a function of stripe width. © 2009 The Japan Society of Applied Physics

**DOI:** 10.1143/JJAP.48.04C120

## 1. Introduction

Lasers based upon the GaAs materials system offer a number of advantages over their InP counterparts, namely the use of larger substrates (>3 in.) for reduced fabrication costs, and a larger conduction band offset enabling higher temperature (or uncooled) operation through improved carrier confinement. Recent developments, such as high quality dilute nitride quantum wells (QW)s,[1] and InAs quantum dots at 1.3 μm[2] have brought about the commercialization of GaAs based optical communications devices. GaAs edge emitting lasers are typically only available commercially as Fabry–Pérot ridge or oxide stripe structures. Such structures, whilst simple, suffer from surface recombination, carrier spreading, and poor fibre coupling efficiencies. Buried heterostructures and self-aligned stripes are typically utilized in the manufacture of InP telecomms lasers yielding devices with: high reliability; small active widths; high quality interfaces; reduced non-radiative recombination at exposed surfaces; and control of carrier flow permitting high local current densities for low drive currents, allowing the use of inexpensive drive electronics. Additionally, the flexibility provided by this approach affords narrower and more symmetric far field emission profiles allowing more efficient fibre coupling.

Epitaxial regrowth in GaAs-based structures is problematic, mainly due to the Al-containing layers within the structure which, when exposed to oxygen, result in poor regrowth interfaces, deleterious to the laser performance. Previous solutions have included the use of: Al-free epitaxial structures;[3] steam oxidation for current confinement;[4] *in-situ* etching and regrowth within a metal organic vapour phase epitaxy (MOVPE) reactor;[5] and antiguided[6] or buried ridge[7] structures where Al layers were exposed to oxygen. True buried heterostructures devices utilising InGaP cladding layers have been realised,[8] but this is problematic due to the need to precisely control the InGaP lattice constant and thus removes the ability to decrease the vertical beam divergence.[9] All these have associated difficulties in process control, reliability, and design flexibility.

We have previously reported a novel technique for the fabrication of GaAs-based self-aligned lasers utilising a lattice matched n-doped InGaP current blocking layer which also provides optical confinement via predominantly index guiding.[10] In this paper we present external quantum differential efficiency, characteristic temperature and far field measurements as a function of stripe width of these devices. This technology relies upon the careful design of the epitaxial structure to ensure no $Al_xGa_{1-x}As$ is exposed during the fabrication process. We combine these ideas in a device structure to avoid issues with oxidising $Al_xGa_{1-x}As$ layers during device processing. In this work we utilise a ~980 nm QW active region design. Such media find widespread application as optical pumps for erbium doped fibre amplifiers. However, the technology would be well suited for exploitation of long wavelength quantum dot and dilute nitride technology for application in metro and access datacomms.

## 2. Device Design and Fabrication

A schematic of the device is shown in Fig. 1(a). Key elements of the design are the refractive index contrasts between the GaAs, AlGaAs, and InGaP in order to provide optical confinement and the p–n–p–n junction formed by the AlGaAs, InGaP, AlGaAs, and GaAs which provides electrical confinement for the stripe region. The modes in the device were modelled using Fimmwave[11] which is a refractive index mode solver. The modelling accounts for refractive index guiding but not for free carrier effects.

The initial MOVPE epitaxial growth was carried out on a 3°-off (100) n+ GaAs substrate. Following the growth of a GaAs buffer, 1000 nm Si-doped $Al_{0.42}Ga_{0.58}As$ (to a concentration of $5 \times 10^{17}$ cm$^{-3}$) lower cladding was grown. The double QW active region is comprised of two $In_{0.17}Ga_{0.83}As$ QWs separated by 20 nm GaAs, grown within a 100 nm GaAs separate confinement heterostructure. Above the active region 300 nm $Al_{0.42}Ga_{0.58}As$ (Zn-doped $5 \times 10^{17}$ cm$^{-3}$) was grown before a 600 nm lattice matched n-doped InGaP layer (Si doped $5 \times 10^{17}$ cm$^{-3}$) was sandwiched between two undoped 10 nm GaAs layers.

The planar wafer was patterned and wet chemically etched (*ex-situ*) into 1, 2, 3, and 5 μm wide stripes. Etching proceeded first with $C_6H_8O_7/H_2O_2$ to selectively etch the GaAs, then $H_3PO_4$/HCl to selectively etch the InGaP, leaving a smooth GaAs surface at the bottom of the stripe. Prior to regrowth the wafer was cleaned in 1% buffered HF. The regrowth process consisted of ramping up to the growth temperature in an arsine environment, before the growth of 100 nm GaAs (C-doped $5 \times 10^{17}$ cm$^{-3}$), 1000 nm $Al_{0.42}Ga_{0.58}As$ (C-doped from $5 \times 10^{17}$ to $1 \times 10^{18}$ cm$^{-3}$), and a 200 nm GaAs contact layer (C-doped $2 \times 10^{19}$ cm$^{-3}$). The material was etched into 50 μm wide ridges for

 © 2009 The Japan Society of Applied Physics

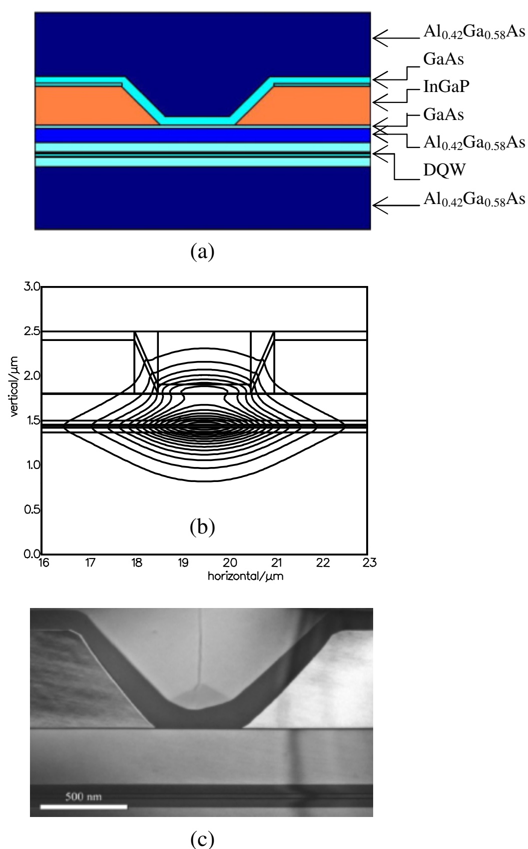


**Fig. 1.** (Color online) (a) Schematic diagram to assist in identifying the layers of the self-aligned stripe. (b) Optical mode as modelled in Fimmwave (only index guiding is considered). (c) Cross-sectional TEM of the regrown structure.

electrical isolation and AuZnAu contact metallization was deposited and annealed at 360 °C. After thinning the substrate InGeAu back contacts were deposited and annealed at 340 °C.

Novel features, which enable this device, are the GaAs layers above and below the InGaP. The upper layer of GaAs is multifunctional: firstly it helps define the etch when the laser stripe is defined and secondly prevents As/P interchange during overgrowth. The lower GaAs acts as an etch stop during the etch procedure thus preventing the underlying AlGaAs being exposed, enabling defect free overgrowth. The thickness and doping concentrations of these layers has been optimised to provide simultaneous optical and electrical confinement. The electrical confinement of carriers requires sufficiently highly doped and thick InGaP whilst the successful confinement of the mode to the active region beneath the InGaP layer requires careful control of the lower GaAs thickness whilst ensuring defect free overgrowth.

A cross-sectional transmission electron micrograph (TEM) of the completed device is shown in Fig. 1(c). This corresponds to a 1 μm wide stripe structure. Comparison with Fig. 1(a) allows identification of the layers. The TEM shows defect free overgrowth and a smooth etch profile of the InGaP. There is a clear compositional variation of the AlGaAs layer which we attribute to growth upon a non-planar surface.[12]

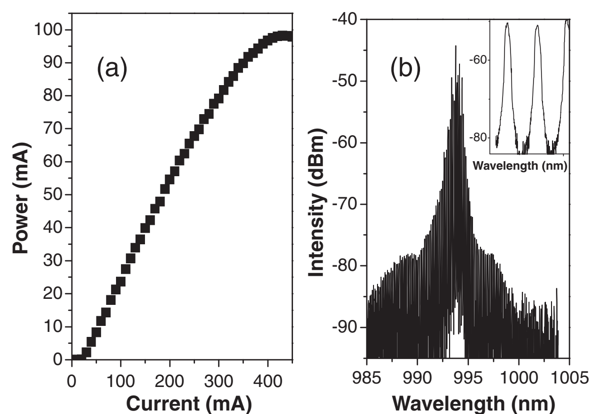


**Fig. 2.** (a) CW output power versus current response of a 3 μm wide stripe laser. Slope efficiency near threshold is 0.316 W A$^{-1}$, corresponding to an external differential quantum efficiency of 50.59%. (b) Lasing spectrum at 40 mA CW.

A light current curve is shown in Fig. 2(a) for a 3 μm stripe laser with a cavity length of 1 mm operated CW at room temperature. The device has a saturated output power of 98 mW caused by thermal roll over of the device. The threshold current is 20 mA corresponding to a threshold current density of 666 A cm$^{-2}$, although this is the upper limit of the threshold current density as zero current spreading has been assumed. Figure 2(b) shows a typical lasing spectrum with a lasing peak at 994 nm. The inset is of two of the Fabry–Pérot modes showing little if any evidence of competing lateral modes.

As further proof of the single lateral mode nature of the emission, the two dimensional near-field profile was scanned using a lensed single mode optical fibre. The measured near-field intensity profile is shown in Fig. 3(a) with black representing zero intensity and pure white the highest intensity. Figure 3(b) plots the horizontal and vertical near-fields extracted from the data which have full width half maximums (FWHM) of 2.8 and 2.2 μm respectively. The resolution of this technique is limited by the spot size of the lensed fibre which we estimate to be ~2–3 μm. Given the resolution limitation this technique demonstrates effective optical confinement within the device.

Figure 4 shows the far field of the devices measured using a Photon Inc. profiling goniometer at a current density of 4 kA cm$^{-2}$. As the ridge width varies from 3 to 5 μm the horizontal far field profile broadens from FWHM of 14.2 to 23.2° consistent with the mode being confined to a narrower stripe width. In the same sense vertical far field FWHM vary from 31.9 to 29.6°, as predicted by modelling using commercial Fimmwave software[11] (not shown), caused by the optical mode being affected by the 100 nm of GaAs grown in the stripe before the AlGaAs, which is more significant in thinner stripe widths.

The external quantum differential efficiency and characteristic temperature are plotted as a function of stripe width in Fig. 5. Maximums for both of these parameters occur for the 2 μm wide stripe. We believe this is due to optimum overlap of the optical mode with the region of the QW which offers gain. This in turn is affected by the injection current confinement (i.e., carriers being efficiently injected in the QWs to provide the gain).

 © 2009 The Japan Society of Applied Physics

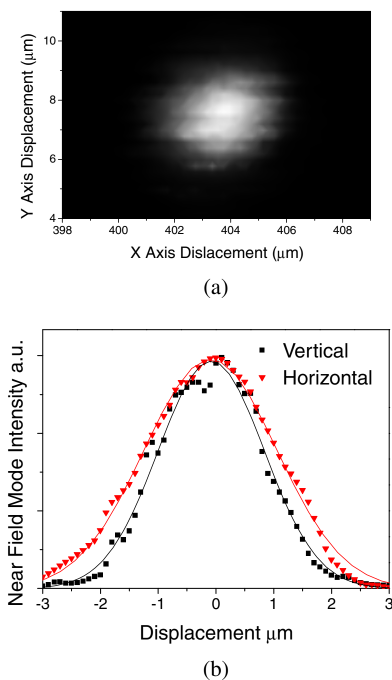


**Fig. 3.** (Color online) (a) Near field intensity profile obtained by scanning a lensed fibre across the laser facet. Black is zero intensity, white is the highest intensity. (b) Extracted horizontal and vertical near field patterns for 1 μm stripe. The resolution limit of this technique is ~2 μm.

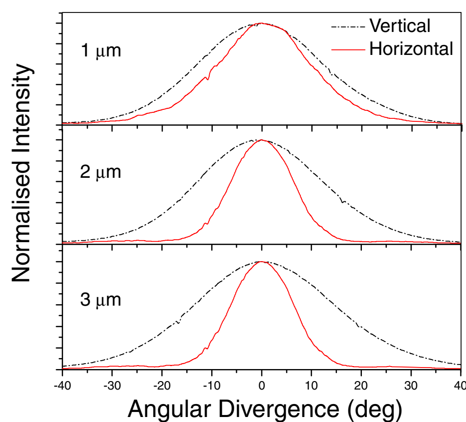


**Fig. 4.** (Color online) Far field profiles for varying ridge widths. The FWHMs are as follows: 1 μm horizontal = 23.2°, vertical = 29.6°; 2 μm horizontal = 30.0°, vertical = 14.25°; 3 μm horizontal = 14.2°, vertical = 31.9°.

## 3. Conclusions

In conclusion, we have presented the operating characteristics for the novel GaAs/InGaP self aligned stripe lasers.

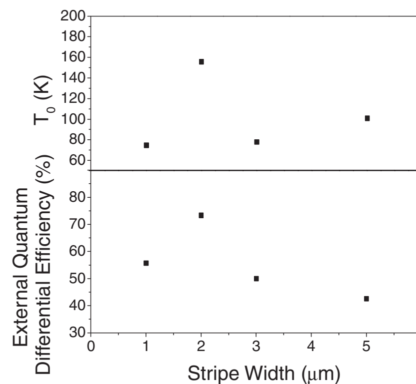


**Fig. 5.** Characteristic temperature ($T_0$) and external differential quantum efficiency ($\eta_d$) given as a function of ridge width. The 2 μm laser demonstrates maximum for both these parameters. The external differential quantum efficiency is taken just above threshold before other high current effects become significant.

We have presented lasing parameters as a function of stripe width, with 2 μm stripes offering the best lasing characteristics in terms of $\eta_d$, $T_0$ and single mode operation at all powers.

## Acknowledgements

This work was supported by the UK Engineering and Physical Sciences Research Council (EPSRC) under Grant EP/E001017/1, and by the Royal Academy of Engineering.

1) N. Tansu, J. Y. Yeh, and L. J. Mawst: IEEE J. Sel. Top. Quantum Electron. **9** (2003) 1220.
2) R. R. Alexander, D. T. D. Childs, H. Agarwal, K. M. Groom, H. Y. Liu, M. Hopkinson, R. A. Hogg, M. Ishida, T. Yamamoto, M. Sugawara, Y. Arakawa, T. J. Badcock, R. J. Royce, and D. J. Mowbray: IEEE J. Quantum Electron. **43** (2007) 1129.
3) N. T. Yeh, W. S. Liu, S. H. Chen, P. C. Chiu, and J. I. Chyi: Appl. Phys. Lett. **80** (2002) 535.
4) F. A. Kish, S. J. Caracci, N. Holonyak, Jr., J. M. Dallesasse, K. C. Hsieh, and M. J. Ries: Appl. Phys. Lett. **59** (1991) 1755.
5) M. Nido, I. Komazaki, K. Kobayashi, K. Endo, M. Ueno, T. Kamejima, and T. Suzuki: IEEE J. Quantum Electron. **23** (1987) 720.
6) L. J. Mawst, H. Yang, M. Nesnidal, A. Al-Muhanna, D. Botez, T. A. Vang, F. D. Alvarez, and R. Johnson: J. Cryst. Growth **195** (1998) 609.
7) S. Ishikawa, K. Fukagai, H. Chida, T. Miyazaki, H. Fujii, and K. Endo: IEEE J. Quantum Electron. **29** (1993) 1936.
8) Y. K. Sin, H. Horikawa, and T. Kamijoh: Electron. Lett. **29** (1993) 240.
9) G. W. Yang, R. J. Hwu, Z. T. Xu, and X. Y. Ma: IEEE J. Quantum Electron. **35** (1999) 1535.
10) K. M. Groom, B. J. Stevens, D. T. Childs, R. R. Alexander, A. B. Krysa, J. S. Roberts, A. S. Helmy, and R. A. Hogg: Electron. Lett. **44** (2008) 905.
11) Fimmwave software by Photon Design [http://www.photond.com].
12) M. Walther, E. Kapon, J. Christen, D. M. Hwang, and R. Bhat: Appl. Phys. Lett. **60** (1992) 521.


© 2009 The Japan Society of Applied Physics